

Visually Lossless Coding in HEVC: A High Bit Depth and 4:4:4 Capable JND-Based Perceptual Quantisation Technique for HEVC

Lee Prangnell

Department of Computer Science, University of Warwick, England, UK

Abstract — Due to the increasing prevalence of high bit depth and YCbCr 4:4:4 video data, it is desirable to develop a JND-based visually lossless coding technique which can account for high bit depth 4:4:4 data in addition to standard 8-bit precision chroma subsampled data. In this paper, we propose a Coding Block (CB)-level JND-based luma and chroma perceptual quantisation technique for HEVC named Pixel-PAQ. Pixel-PAQ exploits both luminance masking and chrominance masking to achieve JND-based visually lossless coding; the proposed method is compatible with high bit depth YCbCr 4:4:4 video data of any resolution. When applied to YCbCr 4:4:4 high bit depth video data, Pixel-PAQ can achieve vast bitrate reductions — of up to 75% (68.6% over four QP data points) — compared with a state-of-the-art luma-based JND method for HEVC named IDSQ. Moreover, the participants in the subjective evaluations confirm that visually lossless coding is successfully achieved by Pixel-PAQ (at a PSNR value of 28.04 dB in one test).

1.0 Introduction

Just Noticeable Distortion (JND)-based visually lossless coding is presently of considerable interest in video coding and image coding research; for example, visually lossless compression is a core consideration in the emerging JPEG-XS still image coding standard. Focusing on video compression in the HEVC standard, JND-based video coding can profoundly reduce the perceptual redundancies that are present in raw YCbCr video data. Therefore, the number of bits required to store each pixel can be considerably reduced without incurring a decrease in the perceptual quality of the reconstructed video data. As such, burdens related to data storage, transmission and bandwidth can be reduced to an extremely high degree. JND is generally defined as the maximum visibility threshold before lossy compression distortions are perceptually discernible to the Human Visual System (HVS) [1, 2]; JND has its roots in the Weber–Fechner law [3]. Even without considering JND, it is well known that raw YCbCr video data, for example, contains a high level of perceptually redundant information. To this end, the HEVC standard [4, 5] includes a multitude of advanced video coding algorithms to achieve high efficiency spatiotemporal compression of raw video data. In the lossy video coding pipeline, spatial image coding (intra-frame coding) and also Group Of Pictures (GOP)-based spatiotemporal video coding (inter-frame coding) are initially employed to dramatically reduce spatiotemporal redundancies typically inherent in all raw video sequences. Intra prediction errors [6] and inter prediction errors [7] produce luma and chroma residual values [8]. The residual values are subsequently transformed into the frequency domain by integer approximations of the Discrete Cosine Transform (DCT) and the Discrete Sine Transform (DST) [9]. The transformed residual values are then quantised using a combination of Rate Distortion Optimised Quantisation (RDOQ) and Uniform Reconstruction Quantisation (URQ) [10]. The DC transform coefficient and the low frequency and medium frequency AC transform coefficients contain the energy which is deemed as the most important in terms of reconstruction quality. Therefore, quantisation is designed to discard the least perceptually important AC coefficients (i.e., the high frequency, or low energy, AC coefficients); the degree to which high frequency AC coefficients are zeroed out is contingent upon the Quantisation Step Size (QStep). Lossless entropy coding of the quantised transform coefficients is performed by the Context Adaptive Binary Arithmetic Coding (CABAC) method; this is the stage at which the actual data compression takes place [11]. If high levels of quantisation are applied, this gives rise to a decrease in non-zero quantised coefficients, which means that the CABAC entropy coder can compress the quantised coefficients more efficiently; that is, the compressed bitstream after entropy coding will contain fewer bits.

With a focused concentration on lossy video coding in the JCT-VC HEVC HM reference codec [12], the video coding algorithms in HEVC HM are based primarily on rate-distortion theory. Consequently, visual quality measurements in HEVC lossy video coding applications are founded upon the Mean Squared Error (MSE) [13]; that is, the MSE of the reconstructed pixel data compared with the raw pixel data. It is a well established fact that the Peak Signal-to-Noise Ratio (PSNR) — which is a logarithmic visual quality metric based on MSE — has a very poor correlation with human visual perception. This is primarily due to the fact that MSE is categorised as a simple statistical risk function; it is often employed in the field of statistics for calculating the average of the squares of the deviations [13]. Therefore, it is considered to be an overly simplistic measuring tool for computing the perceptual quality of compressed video data.

In addition to the primary objective of improving coding efficiency, most lossy video coding algorithms employed in HEVC HM are designed with an emphasis on increasing the PSNR values in the compressed video data. These algorithms include Rate Distortion Optimisation (RDO) [14], RDOQ [15], Deblocking Filter (DF) [16] and Sample Adaptive Offset (SAO) [17]. Note that RDO, RDOQ, DF and SAO are effective methods in terms of increasing PSNR values for the reconstructed video; however, the PSNR-based mathematical reconstruction quality improvement attained by these techniques is perceptually negligible in terms of how the human observer interprets the perceived quality of the compressed video data. For instance, several studies have shown that a compressed video with a PSNR measure of 40 Decibels (dB), or above, typically constitutes visually lossless coding. That is, a coded video with a $\text{PSNR} \geq 40 \text{ dB}$ is perceptually indistinguishable from the raw video data. Furthermore, using the example of $\text{PSNR} \geq 40 \text{ dB}$ for visually lossless coding, this also implies that targeting a reconstruction quality of $\text{PSNR} > 40 \text{ dB}$ (e.g., $\text{PSNR} = 50 \text{ dB}$) is superfluous; i.e., unnecessary bits would be wasted by achieving the superior mathematical reconstruction quality required for the $\text{PSNR} = 50 \text{ dB}$ measurement.

The key difference between JND-based video coding and video coding based on rate-distortion theory is as follows: JND techniques prioritise, above all else, the human observer with respect to assessing the reconstruction quality of a coded video. That is, instead of focusing purely on mathematically-orientated visual quality metrics including PSNR. This is because, in the end, the human observer is the ultimate judge of the visual quality of a compressed video sequence. As such, human subjective quality evaluations are critically important in terms of assessing the reconstruction quality of video sequences coded by JND-based methods. JND techniques are primarily concerned with the following core objective: To reduce bitrates, as much as possible (i.e., reduce the number of bits required to store each pixel), without incurring a perceptually discernible decrease in the compressed video data. Note that with JND and visually lossless coding, PSNR measurements are not considered to be important in terms of quantifying the perceptual quality of a reconstructed sequence. In such cases, the PSNR metric is utilised for quantifying the degree to which PSNR values can be decreased before the associated compression-induced distortions in the coded video are perceptually discernible.

The vast majority of JND techniques in video compression applications target the spatiotemporal domain, the frequency domain or a combination of the two. Mannos' and Sakrison's pioneering work in [18] formed a useful foundation for all frequency domain luminance Contrast Sensitivity Function (CSF)-based JND techniques which target HVS-based redundancies in luminance image data. Chou's and Chen's pioneering pixel-wise JND method in [19, 20] formed the basis for several spatiotemporal domain JND contributions. The primary means by which Chou and Chen achieved pixel-wise JND are luminance-based spatial masking, contrast masking and temporal masking.

1.1 Overview of Related Work

In [21], Ahuma and Peterson devise the first DCT-based JND technique, in which a luminance spatial CSF is incorporated. In [22], Watson expands on Ahuma's and Peterson's work by incorporating luminance masking and contrast masking into the spatial CSF (in the frequency domain); note that power functions corresponding to Weber's law are utilised in this method. Chou and Chen develop a pioneering pixel-wise JND profile in [19], in which luminance masking and contrast masking functions are proposed for utilisation in the spatial domain (8-bit precision luma component). This method is based on average background luminance and also luminance adaptation. The authors further expand on this method in [20] by adding a temporal masking component, in which inter-frame luminance is exploited. Yang et al. in [23] propose a pixel-wise JND contribution to eradicate the overlapping effect between luminance masking and contrast masking effects. This technique also includes a filter for motion-compensated residuals, in which they employ a modified version of Chou's and Chen's spatiotemporal domain JND methods. In [24], Jia et al. present a DCT-based JND technique based on a CSF-based temporal masking effect. Wei and Ngan in [25] introduce a novel DCT-based JND method for video coding, in which the authors incorporate luminance masking, contrast masking and temporal masking effects into the technique. The luminance masking component is modelled as a piecewise linear function. The contrast masking aspect is contextualised as edge and texture masking; the temporal masking component quantifies temporal frequency by taking into account motion direction. Chen and Guillemot in [26] propose a spatial domain foveated masking JND technique, which is the first time that image fixation points are taken into account in JND modelling. Moreover, this method also incorporates the luminance masking, contrast masking and temporal masking functions from Chou's and Chen's methods in [19, 20]. In [27], Naccari and Mrak propose a JND-based perceptual quantisation method (named IDSQ) which exploits luminance CSF-related spatial masking. IDSQ exploits the decreased perceptual sensitivity of the HVS to quantisation-induced compression artifacts in areas within YCbCr video data that contain high and low luma sample intensities. Zhang et al. in [28] expand on Naccari's and Mrak's IDSQ technique by applying it to High Dynamic Range (HDR)-related tone-mapping applications.

As is evident in the overwhelming vast majority of JND contributions that have been previously proposed, the JND of chrominance data is neglected. That is, all of the proposed JND techniques highlighted in sub-section 1.1 focus exclusively on luminance-based JND. Many of these methods share one or more of the same features included in previously proposed JND techniques, which are as follows: luminance masking, luminance-based contrast masking, luminance-based temporal masking and luminance-based CSF. As such, if the corresponding JND techniques were to be applied to contemporary video coding applications, the JND threshold for chrominance data is treated as identical to the JND threshold for luminance data. This is a major drawback because chrominance data is considerably different from luminance data. Therefore, this leaves a research gap in the literature; i.e., it is important and desirable to develop a comprehensive JND method that accounts for both luminance and chrominance data. In addition to the absence of accounting for chrominance JND, other issues exist that are not considered in contemporary pixel domain JND techniques. For example, the method proposed by Yang et al. in [23] and also the method proposed by Chen and Guillemot both employ the luminance masking and contrast masking functions derived by Chou's and Chen's techniques in [19, 20]. The issue here is as follows: the psychophysical experiments undertaken by Chou and Chen — to derive empirical parameter values for the luminance and contrast masking functions — were conducted in 1995-96 on obsolete visual display technologies. The authors who have adopted Chou's and Chen's luminance masking and contrast masking functions have not taken into account the fact that contemporary visual display technologies (e.g., 55 inch Ultra HD-capable, high bit depth-capable and YCbCr 4:4:4-capable LED TVs and monitors) are considerably different compared with obsolete, SD and low resolution CRT monitors.

Another potential issue with previously proposed JND methods — with the exception of Zhang’s HDR-related tone-mapping extension [28] of Naccari’s and Mrak’s JND-based IDSQ technique — is the fact that they are designed for raw 24-bit YCbCr data (i.e., 8-bits per channel data). This equates to the fact that most of the aforementioned empirical parameters in the luminance masking, contrast masking and temporal masking functions are designed to work with 8-bit precision data only. This may prove to be a significant issue because high bit depth data (i.e., up to 16-bits per channel data) is becoming increasingly popular in current video and image applications. Due to the increasing utilisation of 4:4:4 video data which comprise high bit depth, HD and Ultra HD characteristics, the perceptual video coding of all colour channels in such data is desirable. As per the literature review, there is presently a gap in the literature. There is an absence of a JND technique which accounts for: 1) Both the luminance channel and the chrominance channels; 2) The bit depth of raw video data — e.g., 8-bit, 10-bit, 12-bit and 16-bit YCbCr data; and 3) Evaluations on full chroma sampling video data (i.e., YCbCr 4:4:4) in addition to chroma subsampled data (i.e., YCbCr 4:2:0 and 4:2:2).

In this paper, a CB-level JND-based luma and chroma perceptual quantisation technique (named Pixel-PAQ) is proposed for HEVC. Pixel-PAQ is designed to perceptually increase the Y QP, the Cb QP and the Cr QP at the CB level in HEVC; this approach facilitates the JND-based perceptual coding of both luma and chroma data. One significant feature of Pixel-PAQ is that it extends Naccari’s and Mrak’s JND-based IDSQ technique in [27]; that is, the JND for chrominance data is accounted for in Pixel-PAQ (as opposed to luminance data only, which is the case with IDSQ). Accordingly, the proposed technique exploits both luminance masking and chrominance masking based on spatial CSF-related luminance adaptation and chrominance adaptation. In relation to the perceptual coding of chroma Cb and Cr data, Pixel-PAQ has the potential to considerably outperform Naccari’s and Mrak’s JND-based IDSQ technique in terms of bitrate reductions. According to the aforementioned chrominance CSF-related functions, Pixel-PAQ is designed to apply coarser levels of quantisation to Cb and Cr data when coding YCbCr 4:4:4 data and also 4:2:0, 4:2:2 and chroma subsampled data. The proposed method is particularly effective when applied to high bit depth YCbCr 4:4:4 video data, primarily because the Cb and Cr channels in high bit depth 4:4:4 data typically contain a considerable amount of perceptual redundancy due to the higher variances in the chroma channels. Moreover, compression artifacts in high variance chroma data are not conspicuous to the HVS. Therefore, the Cb and Cr data in high bit depth YCbCr 4:4:4 video sequences can be compressed much more aggressively than the Y data.

The rest of this paper is organised as follows. Section 2 includes detailed technical information on the proposed Pixel-PAQ method. Section 3 includes the evaluation, results and discussion of the proposed technique. Finally, section 4 concludes the paper.

2.0 Pixel-PAQ: JND-Based Luminance and Chrominance Perceptual Quantisation

Pixel-PAQ extends Naccari’s and Mrak’s spatial CSF-related and luminance adaptation-based IDSQ JND technique in [27]. Unlike the HDR-related tone-mapping extension of this method in [28], Pixel-PAQ focuses on extending IDSQ to incorporate chrominance JND in addition to accounting for high bit depth luma data and high bit depth chroma data. Both luminance masking and chrominance masking piecewise functions are employed to perceptually increase quantisation levels by virtue of JND-based modifications to the luma QStep and the chroma QSteps at the CB level. A primary objective of Pixel-PAQ is to decrease the number of perceptually insignificant non-zero luma and chroma transform coefficients. This equates to the fact that, after entropy coding, the resulting coded bitstream will contain significantly fewer bits, thus reducing bitrate and non-volatile data storage requirements. The coarser quantisation noise induced by Pixel-PAQ is indiscernible to the human observer assuming that the luma and chroma JND visibility thresholds are not exceeded.

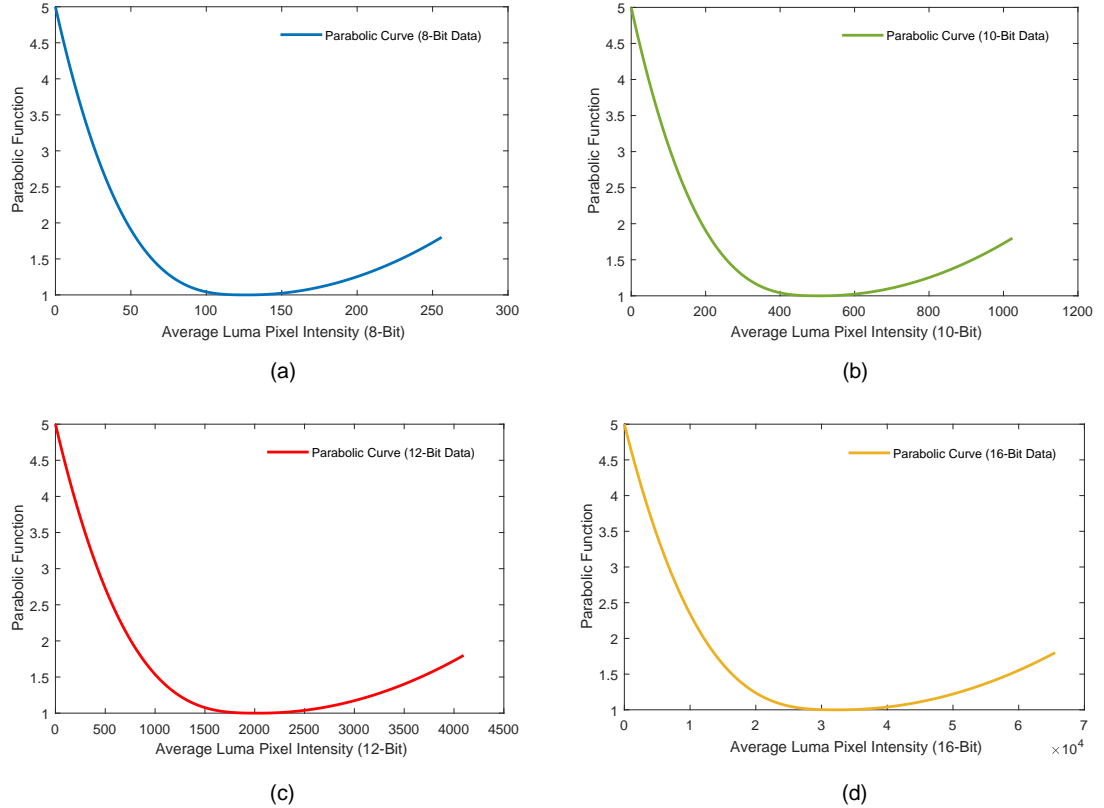


Figure 1. The curves derived from the parabolic function $L(\mu_Y)$ in (1). Note that the subfigures are as follows: (a) corresponds to the parabolic curve when $b = 8$ (8-bit luma data), (b) $b = 10$ (10-bit luma data), (c) $b = 12$ (12-bit luma data) and $b = 16$ (16-bit luma data). Note how, regardless of the bit depth of the luma data, the integrity of the parabolic curve is preserved.

Naccari's and Mrak's JND-based IDSQ method in [27] is founded upon the DCT-based JND technique proposed by Zhang et al. in [29]. In [29], Zhang et al. conclude that there is an intrinsic relationship between luminance adaptation, background luminance and the corresponding luma data in an image. Concerning luminance adaptation, the authors of [29] assert that the contrast threshold for luminance exhibits a parabolic curve corresponding to CSF-related grey level luminance, from which a parabolic piecewise function is derived. Naccari and Mrak employ this piecewise function and recontextualise it for application in HEVC.

2.1 JND-Based Luminance Perceptual Quantisation

In Pixel-PAQ, the adoption of the aforementioned parabolic piecewise function which also constitutes the luma JND visibility threshold, denoted as $L(\mu_Y)$, is utilised as a weight to perceptually increase the luma QStep in HEVC. Function $L(\mu_Y)$ is computed in (1):

$$L(\mu_Y) = \begin{cases} a \cdot \left(1 - \frac{2\mu_Y}{2^b}\right)^d + 1, & \text{if } \mu_Y \leq \frac{2^b}{2} \\ c \cdot \left(\frac{2\mu_Y}{2^b} - 1\right)^f + 1, & \text{otherwise} \end{cases} \quad (1)$$

where parameters a , c , d and f are set to values 2, 0.8, 3 and 2, respectively. These parameter values are selected by Zhang et al. in [29] to determine the shape of the spatial CSF-related luminance adaptation parabolic curve (see Figure 1). Recall that Naccari and Mrak adopt (1) in their IDSQ technique [27].

Zhang et al. in [29] approximate the shape of the parabola, as shown in Figure 1 (a), based on the luminance spatial CSF psychophysical experiments conducted by Ahumada and Peterson in [21]. Note that the parabolic curve is a horizontally and vertically inverted version of the well established luminance CSF and spatial frequency parabolic curve. In Pixel-PAQ, the value 256 in (1) is replaced by 2^b , where superscript b denotes the bit depth of the raw sample data in a luma CB; this is to ensure that the proposed method is compatible with luma data of any bit depth. Furthermore, the integrity of the parabolic curve, as shown in Figure 1, is preserved regardless of the value of b (i.e., the bit depth of the luma data) in (1). Assuming that value 256 in (1) is replaced with 2^b , $L(\mu_Y)$ can subsequently be utilised in perceptual quantisation techniques for luma data of any bit depth. Furthermore, it is important to note that the mean values for the full range of luma data for any bit depth — i.e., $(0+256/2)$ for 8-bit data, $(0+1024/2)$ for 10-bit data, $(0+4096/2)$ for 12-bit data and $(0+65536/2)$ for 16-bit data — equates to a perceptually identical shade of greyscale colour in the luma component.

In (1), variable μ_Y denotes the mean raw sample value in a luma CB; μ_Y is computed in (2):

$$\mu_Y = \frac{1}{2N \times 2N} \sum_{n=1}^{2N \times 2N} w_{Y_n} \quad (2)$$

where $2N \times 2N$ denotes the number of sample values in a luma CB and where variable w_{Y_n} refers to the n^{th} sample value in a luma CB. To reiterate, we compute μ_Y from the original, raw sample values at the luma CB level.

There is a binary logarithmic relationship between the QP and the QStep in URQ in HEVC; this is the case for both slice-level and CB-level luma and chroma quantisation. In the luminance JND aspect of Pixel-PAQ, the primary objective is to perceptually increase the luma QStep by weighing it with $L(\mu_Y)$. In URQ in HEVC, the luma QP (denoted as QP_Y) and the luma QStep (denoted as $QStep_Y$) are computed in (3) and (4), respectively.

$$QP_Y(QStep_Y) = \lceil 6 \times \log_2(QStep_Y) \rceil + 4 \quad (3)$$

$$QStep_Y(QP_Y) = 2^{\frac{QP_Y - 4}{6}} \quad (4)$$

The quantisation-induced error after the reconstruction of the luma data (denoted as q_Y) is only perceptually discernible if it exceeds the luma JND visibility threshold $L(\mu_Y)$. Visually lossless coding is therefore achieved if $|q_Y| \leq L(\mu_Y)$.

To reiterate, the luma QStep that incurs the maximum amount of perceptually indiscernible quantisation-induced distortion is achieved by adaptively weighing $QStep_Y$ with $L(\mu_Y)$. Therefore, the CB-level JND-based perceptual luma QStep, denoted as $PStep_Y$, is quantified in (5).

$$PStep_Y = QStep_Y \cdot [L(\mu_Y)] \quad (5)$$

Accordingly, the CB-level JND-based perceptual luma QP, denoted as PQP_Y , is computed in (6).

$$PQP_Y(PStep_Y) = \lceil 6 \times \log_2(PStep_Y) \rceil + 4 \quad (6)$$

2.2 JND-Based Chrominance Perceptual Quantisation

In [30], Naccari and Pereira propose a JND-based quantisation matrix technique for the Advanced Video Coding (AVC) standard. In this work, the authors assert that perceptual masking is similar for both luma and chroma components data on assumption that the corresponding spatial CSFs for exhibit similar properties. Therefore, Naccari and Pereira in [30] apply the same JND threshold for both luma and chroma quantisation. Although the luminance spatial CSF and the chrominance spatial CSF share somewhat similar properties [31], there are obvious differences between the two, especially in relation to the comparative sensitivity of the HVS to achromatic data and chromatic data in compressed video data [32, 33].

In Pixel-PAQ, a relatively similar piecewise function to (1) is utilised for the CB-level JND-based perceptual quantisation of chroma Cb and Cr data. The corresponding chrominance piecewise functions, denoted as $C_{Cb}(\mu_{Cb})$ and $C_{Cr}(\mu_{Cr})$, are based on chrominance adaptation related to chrominance spatial CSF. The mean values of $C_{Cb}(\mu_{Cb})$ and $C_{Cr}(\mu_{Cr})$ are denoted as μ_{Cb} and μ_{Cr} , respectively, which are utilised to perceptually weigh the chroma QSteps. Functions $C_{Cb}(\mu_{Cb})$ and $C_{Cr}(\mu_{Cr})$, which constitute the chroma Cb and Cr JND visibility thresholds, are computed in (7) and (8), respectively:

$$C_{Cb}(\mu_{Cb}) = \begin{cases} \frac{-\mu_{Cb} \cdot (g-1)}{h+g} & \text{if } \mu_{Cb} \leq h \\ 1 & \text{if } h < \mu_{Cb} < j \\ \frac{(\mu_{Cb} - j) \cdot (h-1)}{(2^b - 1 - j) + 1} & \text{otherwise} \end{cases} \quad (7)$$

$$C_{Cr}(\mu_{Cr}) = \begin{cases} \frac{-\mu_{Cr} \cdot (g-1)}{h+g} & \text{if } \mu_{Cr} \leq h \\ 1 & \text{if } h < \mu_{Cr} < j \\ \frac{(\mu_{Cr} - j) \cdot (h-1)}{(2^b - 1 - j) + 1} & \text{otherwise} \end{cases} \quad (8)$$

where parameters g , h , j and k are set to values 3, 85, 90 and 3, respectively. Similar to the way in which Naccari and Mrak adopt parameter values a , c , d and f in (1) for IDSQ (i.e., based on the luminance spatial CSF-based psychophysical experiments conducted by Zhang et al. in [29]), the values for parameters g , h , j and k in Pixel-PAQ are selected based on the chrominance adaptation psychophysical experiments conducted by Wang et al. in [32]. In [32], the authors conduct chrominance spatial CSF-based psychophysical experiments, from which the values for g , h , j and k are derived; these parameter values are adopted for utilisation in Pixel-PAQ. Note that the data in the chroma Cb and Cr channels exhibit very similar spatial properties [32, 33]; therefore, parameter values g , h , j and k are employed in both (7) and (8), respectively. Variables μ_{Cb} and μ_{Cr} denote the mean raw chroma sample values in chroma Cb and Cr CBs, respectively; they are computed in (9) and (10), respectively:

$$\mu_{Cb} = \frac{1}{M} \sum_{m=1}^M h_{Cb_m} \quad (9)$$

$$\mu_{Cr} = \frac{1}{M} \sum_{m=1}^M s_{Cr_m} \quad (10)$$

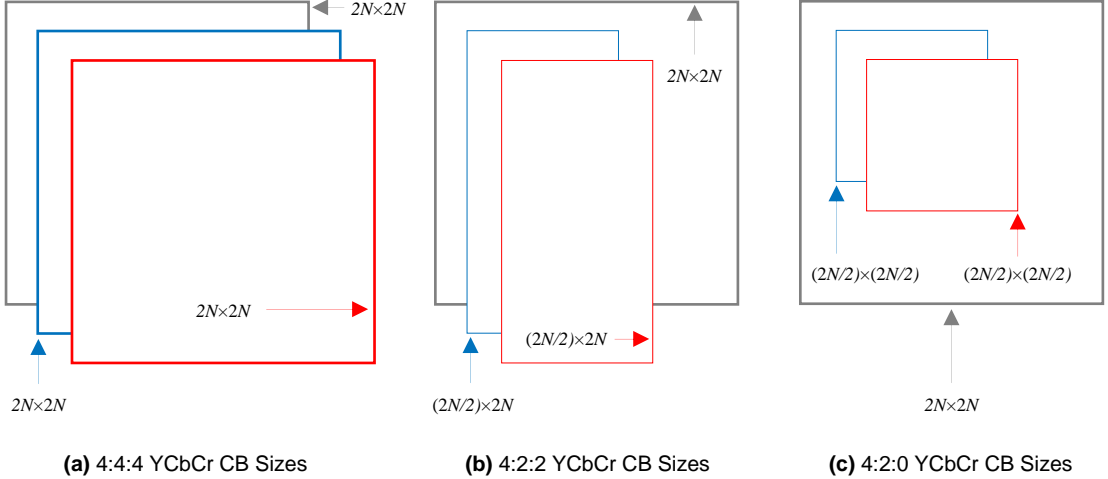


Figure 2. The sizes of Y, Cb and Cr CBs in a $2N \times 2N$ CU in HEVC: Y (grey), Cb (blue), Cr (red). Each subfigure specifies the size of Cb and Cr CBs for different raw video data: (a) for 4:4:4 YCbCr video data, the CB sizes for Y, Cb and Cr are all $2N \times 2N$, (b) for YCbCr 4:2:2 video data, the CB sizes are as follows: $Y_{CB} = 2N \times 2N$, $Cb_{CB} = (2N/2) \times 2N$ and $Cr_{CB} = (2N/2) \times 2N$. (c) for YCbCr 4:2:0 video data, the CB sizes are as follows: $Y_{CB} = 2N \times 2N$, $Cb_{CB} = (2N/2) \times (2N/2)$ and $Cr_{CB} = (2N/2) \times (2N/2)$.

where M denotes the number of sample values in the chroma Cb and Cr CBs, variable h_{Cb} refers to the m^{th} sample value in a Cb CB and variable s_{Cr} refers to the m^{th} sample value in a Cr CB. Unlike the number of sample values in Y CBs, and also due to potential chroma subsampling, M is not a fixed value. Moreover, note that Cb and Cr CBs are always identical in size regardless of the chroma sampling ratio (e.g., 4:4:4, 4:2:2 or 4:2:0) — see Figure 2. As is the case with QP_Y and $QStep_Y$ in (3) and (4), respectively, in URQ there is a binary logarithmic relationship between the chroma Cb and Cr QPs (denoted as QP_{Cb} and QP_{Cr} , respectively) and the chroma Cb and Cr QSteps (denoted as $QStep_{Cb}$ and $QStep_{Cr}$, respectively). Accordingly, QP_{Cb} , $QStep_{Cb}$, QP_{Cr} and $QStep_{Cr}$ are computed in (11)-(14), respectively:

$$QP_{Cb}(QStep_{Cb}) = \lceil 6 \times \log_2(QStep_{Cb}) \rceil + 4 \quad (11)$$

$$QStep_{Cb}(QP_{Cb}) = 2^{\frac{QP_{Cb}-4}{6}} \quad (12)$$

$$QP_{Cr}(QStep_{Cr}) = \lceil 6 \times \log_2(QStep_{Cr}) \rceil + 4 \quad (13)$$

$$QStep_{Cr}(QP_{Cr}) = 2^{\frac{QP_{Cr}-4}{6}} \quad (14)$$

Recall that the HVS is significantly more sensitive to spatial contrast in luminance data compared with the corresponding spatial contrast sensitivity response to chromatic data. This correlates with the well established fact that the HVS is considerably less sensitive to gradations — including quantisation-induced compression artifacts — in compressed chroma data. This is the main reason why chrominance data can be quantised much more aggressively, especially high variance chroma data. To reiterate, quantisation-induced compression artifacts are vastly more perceptible in reconstructed luma data; this is primarily due to the fact that the luma channel contains all of the fine details in YCbCr pictures [34].

The quantisation-induced errors after the reconstruction of chroma Cb and Cr data, denoted as q_{Cb} and q_{Cr} , respectively, are perceptually discernible if they exceed the chroma Cb and Cr JND visibility thresholds $C_{Cb}(\mu_{Cb})$ and $C_{Cr}(\mu_{Cr})$, respectively. Visually lossless coding is achieved if $|q_{Cb}| \leq C_{Cb}(\mu_{Cb})$ and $|q_{Cr}| \leq C_{Cr}(\mu_{Cr})$.

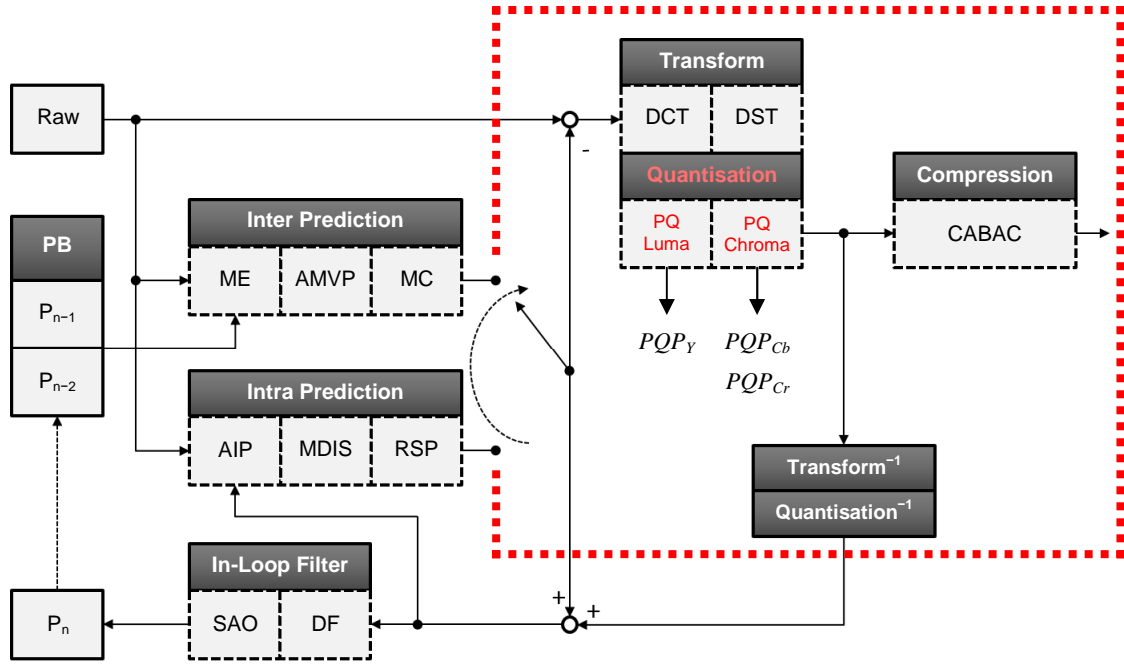


Figure 3. A block diagram which shows the proposed Pixel-PAQ method implemented into the JCT-VC HEVC HM encoder. The red dotted line and the red text indicate the areas within the HEVC coding pipeline in which the proposed method is implemented. Note that variables PQP_Y , PQP_{Cb} and PQP_{Cr} denote the perceptually adaptive QPs.

To achieve the JND-based perceptual quantisation of chroma Cb and Cr data, $QStep_{Cb}$ and $QStep_{Cr}$ are weighed with μC_{Cb} and μC_{Cr} , respectively. The chroma perceptual QSteps and QPs, denoted as $PStep_{Cb}$, $PStep_{Cr}$, PQP_{Cb} and PQP_{Cr} , are computed in (15)-(18), respectively.

$$PStep_{Cb} = QStep_{Cb} \cdot [\mu C_{Cb}] \quad (15)$$

$$PQP_{Cb}(PStep_{Cb}) = [6 \times \log_2(PStep_{Cb})] + 4 \quad (16)$$

$$PStep_{Cr} = QStep_{Cr} \cdot [\mu C_{Cr}] \quad (17)$$

$$PQP_{Cr}(PStep_{Cr}) = [6 \times \log_2(PStep_{Cr})] + 4 \quad (18)$$

In relation to the initial QPs utilised to evaluate Pixel-PAQ (i.e., QPs 22, 27, 32 and 37), the proposed method is implemented into HEVC HM by exploiting the CB-level chroma Cb and Cr QP offset signalling mechanism provided by JCT-VC [35, 36]. Therefore, the Cb and Cr QPs are perceptually increased at the CB level by offsetting them against PQP_Y . These QP and QStep offsets, denoted as OQP_{Cb} , $OStep_{Cb}$, OQP_{Cr} and $OStep_{Cr}$, respectively, are quantified in (19)-(22).

$$OQP_{Cb}(\mu C_{Cb}) = PQP_Y + [3\mu C_{Cb}] \quad (19)$$

$$OStep_{Cb}(\mu C_{Cb}) = 2^{\frac{PQP_Y + [3\mu C_{Cb}] - 4}{6}} \quad (20)$$

$$OQP_{Cr}(\mu C_{Cr}) = PQP_Y + [3\mu C_{Cr}] \quad (21)$$

$$OStep_{Cr}(\mu C_{Cr}) = 2^{\frac{PQP_Y + [3\mu C_{Cr}] - 4}{6}} \quad (22)$$

In relation to the aforementioned CB-level chroma Cb and Cr QP offset signalling technique present in the latest versions of JCT-VC HEVC HM [35, 36], this method is also exploited in our previously published perceptual quantisation contribution named FCPQ [37]. That is, we exploit the flexibility provided by JCT-VC in terms of signalling to the decoder — in the Picture Parameter Set (PPS) — chroma QP offsets at the CB level. The signalling of CB-level Cb and Cr QP offsets in the PPS proved to be particularly advantageous for FCPQ, primarily because it allows for a straightforward encoder side implementation (see Figure 3). In essence, by employing this chroma QP offset scheme, all of the CB-level quantisation-related data can be efficiently transmitted to the decoder; this ensures that the perceptually compressed video is correctly decoded and reconstructed. Furthermore, the mean raw Y, Cb and Cr sample values can be accounted for without affecting coding efficiency and computational complexity.

3.0 Evaluation, Results and Discussion

Pixel-PAQ is evaluated and compared with Naccari's and Mrak's JND-based IDSQ technique in [27], which has been previously proposed for the HEVC standard. It is important to affirm that IDSQ has been shown to significantly outperform both URQ and RDOQ [27] (i.e., the default scalar quantisation techniques in HEVC); furthermore, RDOQ is disabled in all tests. Pixel-PAQ is implemented into JCT-VC HEVC HM 16.7 and the method is tested on 18 official JCT-VC test sequences; namely, the proposed method is evaluated on the YCbCr 4:2:0, 4:2:2 and 4:4:4 versions of BirdsInCage, DuckAndLegs, Kimono, OldTownCross, ParkScene and Traffic. All of these sequences comprise a spatial resolution of HD 1080p (1920×1080). The 4:4:4 and 4:2:2 versions of these sequences contain a higher dynamic range (i.e., 10-bits per pixel per channel, which equates to 30-bits per pixel), whereas the 4:2:0 versions comprise 8-bits per pixel per channel. In our previously published work in [37], we provide empirical evidence that an absence of chroma subsampling in addition to a higher dynamic range for each colour channel are significantly advantageous for the perceptual quantisation of YCbCr data; this is particularly pertinent to 4:4:4 data. Therefore, this is the primary reason for employing a similar experimental setup to the one conducted in [37].

Objective visual quality evaluations are undertaken which correspond, as closely as possible, to the Common Test Conditions and Software Reference Configurations recommended by JCT-VC [38]; this is a common experimental setup utilised in contemporary HEVC research for lossy coding techniques. This includes testing techniques with four QP data points (i.e., initial QPs 22, 27, 32 and 37) with the All Intra (AI) and Random Access (RA) encoding configurations [38]. In the objective evaluation, the SSIM [39] and PNSR visual quality metrics are employed to assess the mathematical reconstruction quality of the Pixel-PAQ and IDSQ coded videos.

Due to the fact that both Pixel-PAQ and IDSQ are JND-based and HVS-orientated perceptual video coding techniques, it is of paramount importance to undertake extensive subjective visual quality evaluations in addition to the aforementioned objective visual quality evaluation. As such, the United Nations' ITU-T standardised subjective evaluation procedure entitled *Subjective Video Quality Assessment Methods* (ITU-T P.910 [40]) is employed. In the ITU-T P.910 subjective evaluation, the following conditions are recommended:

- Number of participants ≥ 4 and ≤ 40 ;
- Viewing distance: $1\text{--}8 \times H$, where H is the height of the TV/VDU;
- Compute Mean Opinion Score (MOS);
- Spatiotemporal analysis.

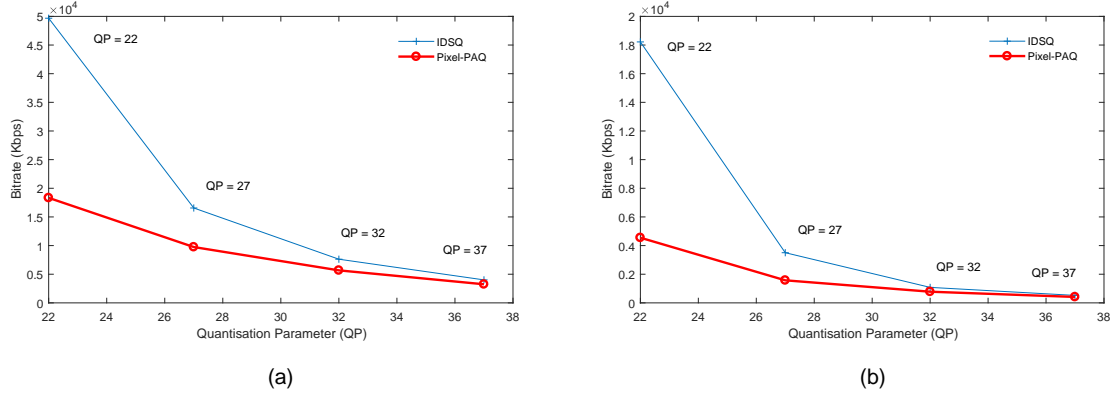


Figure 4. Two plots which highlight the bitrate reductions attained by Pixel-PAQ compared with IDSQ. Subfigure (a) shows the bitrate reductions achieved by Pixel-PAQ on the Kimono 4:4:4 sequence using the AI encoding configuration. Subfigure (b) shows the bitrate reductions achieved by Pixel-PAQ on the BirdsInCage 4:4:4 sequence using the RA encoding configuration.

3.1 Bitrate Reductions and Objective Visual Quality Evaluations

Table 1. Tabulated bitrate reduction percentages attained for the proposed Pixel-PAQ technique compared with IDSQ. The bitrate reductions are averaged over four QP data points (i.e., initial QPs 22, 27, 37 and 37). The results are recorded for the YCbCr 4:2:0, 4:2:2 and 4:4:4 versions of the BirdsInCage, DuckAndLegs Kimono, OldTownCross, ParkScene and Traffic sequences using the AI and RA encoding configurations. The AI results are shown on the left; the RA results are shown on the right.

Pixel-PAQ Versus IDSQ (YCbCr 4:2:0) – AI		Pixel-PAQ Versus IDSQ (YCbCr 4:2:0) – RA	
Sequence	Bitrate Reductions (%)	Sequence	Bitrate Reductions (%)
BirdsInCage	-11.0	BirdsInCage	-9.7
DuckAndLegs	-14.0	DuckAndLegs	-10.9
Kimono	-14.3	Kimono	-9.1
OldTownCross	-7.0	OldTownCross	-4.3
ParkScene	-8.3	ParkScene	-5.7
Traffic	-11.0	Traffic	-8.8
Pixel-PAQ Versus IDSQ (YCbCr 4:2:2) – AI		Pixel-PAQ Versus IDSQ (YCbCr 4:2:2) – RA	
Sequence	Bitrate Reductions (%)	Sequence	Bitrate Reductions (%)
BirdsInCage	-25.3	BirdsInCage	-28.7
DuckAndLegs	-30.4	DuckAndLegs	-31.1
Kimono	-31.1	Kimono	-20.1
OldTownCross	-20.7	OldTownCross	-16.9
ParkScene	-27.4	ParkScene	-23.0
Traffic	-15.5	Traffic	-13.9
Pixel-PAQ Versus IDSQ (YCbCr 4:4:4) – AI		Pixel-PAQ Versus IDSQ (YCbCr 4:4:4) – RA	
Sequence	Bitrate Reductions (%)	Sequence	Bitrate Reductions (%)
BirdsInCage	-50.3	BirdsInCage	-68.6
DuckAndLegs	-50.6	DuckAndLegs	-62.9
Kimono	-52.5	Kimono	-43.4
OldTownCross	-48.9	OldTownCross	-56.8
ParkScene	-41.7	ParkScene	-42.8
Traffic	-24.2	Traffic	-26.7

In this sub-section, the bitrate reduction results, in addition to the mathematical reconstruction quality results, are addressed. In the next sub-section the subjective evaluation results are analysed. As shown in the plots in Figure 4 and also in Table 1, Pixel-PAQ achieves exceptional bitrate reduction results on YCbCr 4:4:4 10-bit sequences in comparison with IDSQ. The most outstanding result is achieved on the BirdsInCage 4:4:4 sequence for the initial QP = 22 test using the RA encoding configuration (see Table 1). In this particular test and compared with IDSQ, over 75% bitrate reductions are achieved by Pixel-PAQ; this averages out at 68.6% bitrate reductions over four initial QP values (i.e., QPs 22, 27, 32 and 37). In the RA QP = 22 test, the following bitrate reductions are attained: 4,394.99 Kbps (Pixel-PAQ) versus 17,760.41 kbps (IDSQ) for 600 frames. In terms of data storage requirements on a non-volatile medium, the corresponding final file sizes of the compressed bitstreams are as follows: 5,368 KB (Pixel-PAQ) versus 21,683 KB (IDSQ). Furthermore, the raw BirdsInCage 4:4:4 sequence is 6.95 GB in size and the HEVC mathematically lossless coded version is 2 GB in size; the corresponding Pixel-PAQ coded bitstream is 5.24 MB in size for the RA QP = 22 test. Moreover, in the RA QP = 22 test on this sequence, visually lossless coding is achieved by Pixel-PAQ. That is, based on the Mean Opinion Score (MOS), all four individuals who participated in the subjective evaluations could not discern any perceptible differences between the Pixel-PAQ coded version of the BirdsInCage 4:4:4 sequence and the corresponding raw sequence (the subjective evaluation results are included in sub-section 3.2). This equates to 5.24 MB (Pixel-PAQ) versus 6.95 GB (raw) for identical perceptual quality (compare Figure 5 with Figure 6).



Figure 5. An inter-coded frame (RA QP = 22), coded by Pixel-PAQ, of the BirdsInCage 4:4:4 sequence (visually lossless).



Figure 6. The corresponding frame of the raw BirdsInCage 4:4:4 sequence.



Figure 7. The SSIM Index Map which shows the luma and chroma reconstruction errors in a Pixel-PAQ coded inter-frame (RA QP = 22) of the BirdsInCage 4:4:4 sequence compared with the corresponding frame in the raw sequence.



Figure 8. The SSIM Index Map which shows the luma and chroma reconstruction errors in a Pixel-PAQ coded inter-frame (RA QP = 22) of the BirdsInCage YCbCr 4:4:4 sequence compared with the corresponding IDSQ coded inter-frame.

If we analyse Figure 7 and Figure 8, it is evident that the reconstruction errors are concentrated mostly in the high variance regions of the Y, Cb and Cr data. Due to the high variance-based spatial masking phenomenon of the HVS — as highlighted in our previously published work in [37] — the HVS is less capable of detecting quantisation-induced compression artifacts in high spatial variance regions of compressed luma and chroma data. Therefore, in spite of the reconstruction errors shown in Figure 7 and Figure 8, visually lossless coding is achieved by Pixel-PAQ in both the AI QP = 22 and RA QP = 22 tests on this sequence. It is important to note that visually lossless coding is achieved in virtually all of the sequences tested in the AI QP = 22 and RA QP = 22 experiments; the BirdsInCage 4:4:4 sequence is emphasised because the highest bitrate reductions are achieved by Pixel-PAQ on this sequence.

Table 2. The SSIM results for ‘Pixel-PAQ versus the raw data’ in comparison with ‘IDSQ versus the raw data’ (initial QPs 22, 27, 32 and 37). The results are recorded for the YCbCr 4:2:0, 4:2:2 and 4:4:4 versions of BirdsInCage, DuckAndLegs Kimono, OldTownCross, ParkScene and Traffic sequences using the AI encoding configuration. The Pixel-PAQ results are shown on the left; the IDSQ results are shown on the right.

Mean SSIM Values Per QP: Pixel-PAQ Versus IDSQ (YCbCr 4:2:0) – All Intra								
Sequence	Pixel-PAQ				IDSQ			
	QP 22	QP 27	QP 32	QP 37	QP 22	QP 27	QP 32	QP 37
BirdsInCage	0.9884	0.9852	0.9821	0.9768	0.9907	0.9879	0.9850	0.9813
DuckAndLegs	0.9320	0.9005	0.8765	0.8369	0.9613	0.9195	0.8884	0.8509
Kimono	0.9227	0.9069	0.8926	0.8662	0.9396	0.9235	0.9063	0.8853
OldTownCross	0.9015	0.8534	0.8222	0.7811	0.9157	0.8660	0.8337	0.7958
ParkScene	0.9399	0.9138	0.8803	0.8292	0.9555	0.9302	0.8937	0.8463
Traffic	0.9461	0.9226	0.8953	0.8493	0.9615	0.9411	0.9128	0.8754

Mean SSIM Values Per QP: Pixel-PAQ Versus IDSQ (YCbCr 4:2:2) – All Intra								
Sequence	Pixel-PAQ				IDSQ			
	QP 22	QP 27	QP 32	QP 37	QP 22	QP 27	QP 32	QP 37
BirdsInCage	0.9860	0.9823	0.9763	0.9641	0.9893	0.9860	0.9828	0.9778
DuckAndLegs	0.9021	0.8668	0.8357	0.7911	0.9617	0.9098	0.8610	0.8160
Kimono	0.8990	0.8814	0.8574	0.8128	0.9283	0.9026	0.8836	0.8570
OldTownCross	0.8626	0.8166	0.7762	0.7107	0.9058	0.8362	0.8007	0.7605
ParkScene	0.8682	0.8383	0.8000	0.7430	0.9146	0.8676	0.8308	0.7879
Traffic	0.9506	0.9206	0.8713	0.7864	0.9675	0.9456	0.9111	0.8569

Mean SSIM Values Per QP: Pixel-PAQ Versus IDSQ (YCbCr 4:4:4) – All Intra								
Sequence	Pixel-PAQ				IDSQ			
	QP 22	QP 27	QP 32	QP 37	QP 22	QP 27	QP 32	QP 37
BirdsInCage	0.9790	0.9759	0.9717	0.9653	0.9856	0.9803	0.9761	0.9721
DuckAndLegs	0.8897	0.8396	0.8086	0.7697	0.9709	0.9183	0.8479	0.7924
Kimono	0.8792	0.8635	0.8437	0.8156	0.9279	0.8864	0.8642	0.8407
OldTownCross	0.8001	0.7515	0.7205	0.6823	0.9135	0.8122	0.7391	0.6992
ParkScene	0.8554	0.8268	0.7940	0.7527	0.9212	0.8623	0.8197	0.7774
Traffic	0.9535	0.9282	0.8888	0.8271	0.9686	0.9473	0.9157	0.8682

The size of the bitrate reductions attained by Pixel-PAQ is inversely proportional to the size of the initial QP (see the plots in Figure 4). For instance, recall that the overall bitrate reductions achieved by Pixel-PAQ on the BirdsInCage 4:4:4 sequence averages out at 68.6% over four QP data points (i.e., initial QPs 22, 27, 32 and 37) — see Table 1.

As shown in Table 2 and Table 3, the SSIM [39] objective visual quality results in the Pixel-PAQ versus IDSQ tests are tabulated (AI and RA QP 22, 27, 32 and 37 tests, respectively). In all of the tests conducted to evaluate the efficacy of Pixel-PAQ, the mathematical reconstruction quality (i.e., the SSIM results) of the Pixel-PAQ coded sequences are necessarily inferior to those obtained for the IDSQ coded sequences; this is by virtue of the nature of JND-based perceptual video coding. That is, a higher level of quantisation reduces mathematical reconstruction quality. It is interesting to note that, although SSIM is designed to be more perceptually friendly than PSNR, many of the SSIM results in Table 2 and Table 3 do not correlate with how the participants in the subjective evaluations perceived the visual quality of the reconstructed sequences.

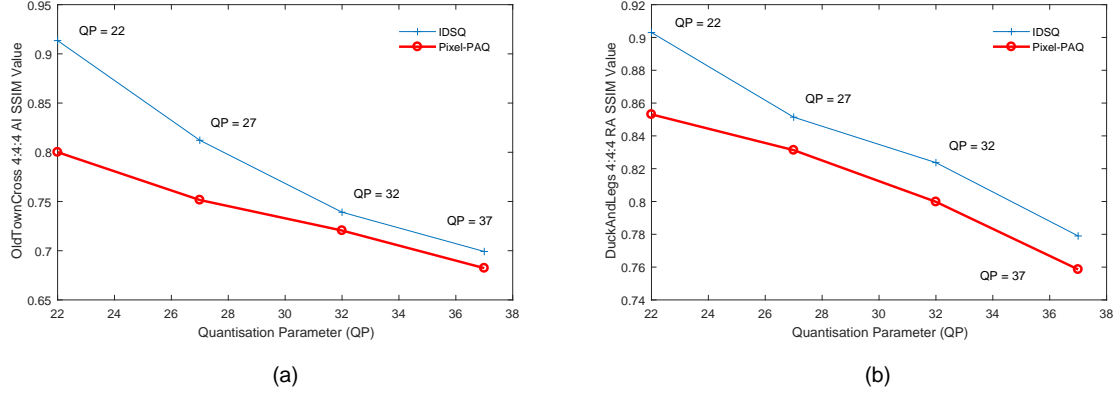


Figure 9. Two plots which highlight the inferior mathematical reconstruction quality of Pixel-PAQ coded sequences versus IDSQ coded sequences, over four QP data points (i.e., QPs 22, 27, 32 and 37), using the SSIM metric. Subfigure (a) shows the results for the OldTownCross 4:4:4 sequence (AI); subfigure (b) shows the results for the DuckAndLegs 4:4:4 sequence (RA).

Table 3. The SSIM results for ‘Pixel-PAQ versus the raw data’ in comparison with ‘IDSQ versus the raw data’ (initial QPs 22, 27, 32 and 37). The results are recorded for the YCbCr 4:2:0, 4:2:2 and 4:4:4 versions of BirdsInCage, DuckAndLegs Kimono, OldTownCross, ParkScene and Traffic sequences using the RA encoding configuration. The Pixel-PAQ results are shown on the left; the IDSQ results are shown on the right.

Mean SSIM Values Per QP: Pixel-PAQ Versus IDSQ (YCbCr 4:2:0) – Random Access

Sequence	Pixel-PAQ				IDSQ			
	QP 22	QP 27	QP 32	QP 37	QP 22	QP 27	QP 32	QP 37
BirdsInCage	0.9883	0.9860	0.9832	0.9782	0.9898	0.9882	0.9857	0.9825
DuckAndLegs	0.9060	0.8897	0.8666	0.8250	0.9196	0.9035	0.8770	0.8381
Kimono	0.9136	0.9002	0.8836	0.8584	0.9251	0.9120	0.8947	0.8749
OldTownCross	0.8565	0.8445	0.8275	0.7930	0.8640	0.8543	0.8374	0.8056
ParkScene	0.9361	0.9112	0.8780	0.8284	0.9480	0.9245	0.8909	0.8459
Traffic	0.9463	0.9267	0.9025	0.8602	0.9573	0.9408	0.9167	0.8838

Mean SSIM Values Per QP: Pixel-PAQ Versus IDSQ (YCbCr 4:2:2) – Random Access

Sequence	Pixel-PAQ				IDSQ			
	QP 22	QP 27	QP 32	QP 37	QP 22	QP 27	QP 32	QP 37
BirdsInCage	0.9856	0.9830	0.9780	0.9673	0.9869	0.9856	0.9831	0.9789
DuckAndLegs	0.8794	0.8591	0.8292	0.7856	0.8954	0.8797	0.8512	0.8065
Kimono	0.8954	0.8766	0.8538	0.8164	0.9016	0.8907	0.8734	0.8492
OldTownCross	0.8171	0.8034	0.7798	0.7324	0.8220	0.8145	0.7977	0.7646
ParkScene	0.8665	0.8421	0.8079	0.7535	0.8816	0.8625	0.8322	0.7919
Traffic	0.9519	0.9276	0.8844	0.8108	0.9634	0.9460	0.9171	0.8693

Mean SSIM Values Per QP: Pixel-PAQ Versus IDSQ (YCbCr 4:4:4) – Random Access

Sequence	Pixel-PAQ				IDSQ			
	QP 22	QP 27	QP 32	QP 37	QP 22	QP 27	QP 32	QP 37
BirdsInCage	0.9777	0.9759	0.9725	0.9666	0.9783	0.9774	0.9756	0.9724
DuckAndLegs	0.8531	0.8313	0.7998	0.7586	0.9030	0.8514	0.8237	0.7790
Kimono	0.8702	0.8574	0.8386	0.8127	0.8761	0.8673	0.8522	0.8316
OldTownCross	0.7504	0.7398	0.7205	0.6868	0.7492	0.7467	0.7326	0.7035
ParkScene	0.8534	0.8303	0.7994	0.7581	0.8637	0.8473	0.8204	0.7825
Traffic	0.9533	0.9322	0.8983	0.8433	0.9620	0.9458	0.9191	0.8771



Figure 10. An intra-coded frame (AI QP = 22), coded by Pixel-PAQ, of the OldTownCross 4:4:4 sequence (visually lossless).



Figure 11. An intra-coded frame (AI QP = 22), coded by IDSQ, of the OldTownCross 4:4:4 sequence.



Figure 12. The corresponding frame of the raw OldTownCross 4:4:4 sequence.

With respect to the objective visual quality SSIM results achieved by Pixel-PAQ coded sequences, the SSIM result attained for the OldTownCross 4:4:4 sequence — AI QP = 22 test — indicates very poor reconstruction quality compared with IDSQ (i.e., 0.8001 versus 0.9135); see Table 2. Furthermore, as confirmed in the subjective evaluations, the perceptual quality of the Pixel-PAQ coded version of this sequence is perceived as visually lossless (see Figures 10-12).

Table 4. The PSNR results for ‘Pixel-PAQ versus the raw data’ in comparison with ‘IDSQ versus the raw data’ (initial QPs 22, 27, 32 and 37). The results are recorded for the YCbCr 4:2:0, 4:2:2 and 4:4:4 versions of BirdsInCage, DuckAndLegs Kimono, OldTownCross, ParkScene and Traffic sequences using the AI encoding configuration. The Pixel-PAQ results are shown on the left; the IDSQ results are shown on the right.

Mean PSNR (dB) Per QP: Pixel-PAQ Versus IDSQ (YCbCr 4:2:0) – All Intra								
Sequence	Pixel-PAQ				IDSQ			
	QP 22	QP 27	QP 32	QP 37	QP 22	QP 27	QP 32	QP 37
BirdsInCage	37.5180	36.0085	34.8799	33.3267	38.8655	37.1534	35.7128	34.2626
DuckAndLegs	31.7584	29.8392	28.6015	26.9424	34.8509	31.3556	29.3250	27.5127
Kimono	35.8659	34.5481	33.5125	31.8994	37.5313	35.9396	34.4053	32.7964
OldTownCross	33.8187	31.8953	30.6139	29.0512	35.0655	32.7264	31.1386	29.5463
ParkScene	34.6698	32.5783	30.7900	28.7431	36.9332	34.0121	31.4805	29.2620
Traffic	35.2647	33.1950	31.5932	29.5243	37.2091	34.8116	32.5567	30.4404

Mean PSNR (dB) Per QP: Pixel-PAQ Versus IDSQ (YCbCr 4:2:2) – All Intra								
Sequence	Pixel-PAQ				IDSQ			
	QP 22	QP 27	QP 32	QP 37	QP 22	QP 27	QP 32	QP 37
BirdsInCage	36.6285	35.2130	33.6314	31.6704	38.2948	36.5251	35.1635	33.6036
DuckAndLegs	30.3503	28.6050	27.2242	25.8192	34.5193	30.7285	28.4722	26.6346
Kimono	35.0233	33.7931	32.3663	30.5674	36.7747	35.2219	33.8264	32.1149
OldTownCross	32.5675	30.9991	29.6107	27.9068	34.4299	31.9390	30.5069	28.9463
ParkScene	32.5660	30.8475	29.2602	27.6884	35.2745	32.7290	30.6848	28.8019
Traffic	34.9795	32.4327	29.9572	27.5877	37.6387	34.6954	31.9075	29.2406

Mean PSNR (dB) Per QP: Pixel-PAQ Versus IDSQ (YCbCr 4:4:4) – All Intra								
Sequence	Pixel-PAQ				IDSQ			
	QP 22	QP 27	QP 32	QP 37	QP 22	QP 27	QP 32	QP 37
BirdsInCage	34.8927	34.0048	33.0221	31.7821	37.2223	35.1969	33.8851	32.8186
DuckAndLegs	29.5754	27.8507	26.6800	25.4676	35.1345	30.5158	27.9026	26.1863
Kimono	34.3420	33.4135	32.2602	30.8592	36.4072	34.5038	33.3406	31.9085
OldTownCross	30.8036	29.7243	28.7834	27.6085	34.0635	30.8971	29.3628	28.1692
ParkScene	32.5565	30.9406	29.4304	27.9728	35.4066	32.7230	30.7505	28.8994
Traffic	35.3045	32.8423	30.4738	28.2057	37.8411	34.8627	32.1028	29.4800

Identical in context to the SSIM results shown in Table 2, and as expected, the PSNR results attained for Pixel-PAQ are inferior to those achieved by IDSQ in all tests (see Table 4 and Table 5). This equates to the fact that both PSNR and SSIM do not correspond to how the Pixel-PAQ coded sequences are visually perceived in realistic viewing situations, as confirmed by the subjective evaluations. As previously mentioned, objective visual quality metrics, including PSNR and SSIM, are employed for an entirely different purpose in perceptually-orientated, visually lossless and JND-based video compression techniques. That is, the main objective is to achieve the largest bitrate reduction possible without incurring a perceptually discernible decrease in reconstruction quality. The human observer is the ultimate judge of visual quality; therefore, the objective visual quality scores, regardless of the metric employed, are somewhat irrelevant. For instance, in the RA QP = 22 test conducted on the DuckAndLegs 4:4:4 sequence, the reconstruction quality measurement achieved, as quantified by PSNR, is approximately 28.04 dB (see Table 5). However, visually lossless coding is still achieved at this extremely low PSNR value.

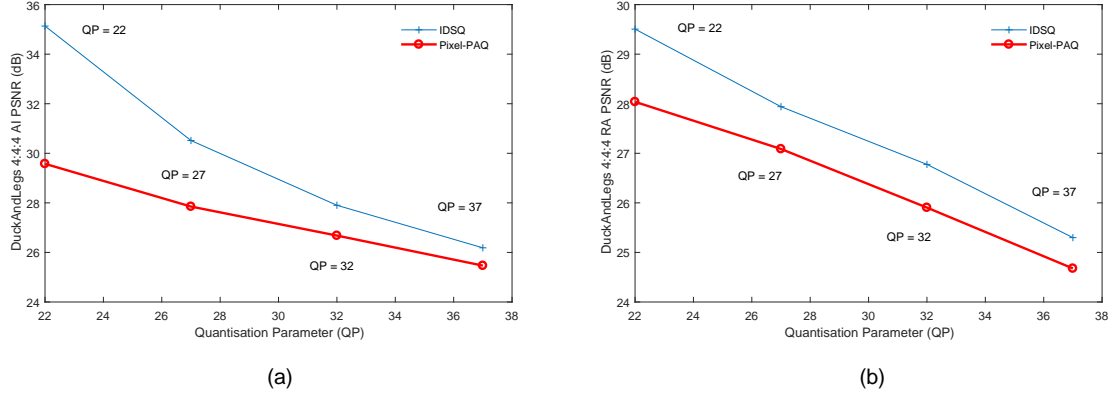


Figure 13. Two plots which highlight the inferior mathematical reconstruction quality of Pixel-PAQ coded sequences versus IDSQ coded sequences, over four QP data points (i.e., QPs 22, 27, 32 and 37), using the PSNR metric. Subfigure (a) shows the results for the DuckAndLegs 4:4:4 sequence (AI); subfigure (b) shows the results for the DuckAndLegs 4:4:4 sequence (RA).

Table 5. The PSNR results for ‘Pixel-PAQ versus the raw data’ in comparison with ‘IDSQ versus the raw data’ (initial QPs 22, 27, 32 and 37). The results are recorded for the YCbCr 4:2:0, 4:2:2 and 4:4:4 versions of BirdsInCage, DuckAndLegs Kimono, OldTownCross, ParkScene and Traffic sequences using the RA encoding configuration. The Pixel-PAQ results are shown on the left; the IDSQ results are shown on the right.

Mean PSNR (dB) Per QP: Pixel-PAQ Versus IDSQ (YCbCr 4:2:0) – Random Access

Sequence	Pixel-PAQ				IDSQ			
	QP 22	QP 27	QP 32	QP 37	QP 22	QP 27	QP 32	QP 37
BirdsInCage	37.3938	36.3239	35.1878	33.6965	38.1668	37.2331	35.9925	34.6063
DuckAndLegs	30.2049	29.0677	27.8971	26.3244	31.4326	30.0737	28.4649	26.8022
Kimono	35.1974	34.0136	32.6811	31.1212	36.2523	34.8071	33.2019	31.6658
OldTownCross	32.3403	31.6902	30.8602	29.4741	32.8560	32.2676	31.3361	29.9690
ParkScene	34.2629	32.4221	30.7282	28.8326	35.7195	33.4312	31.3018	29.3340
Traffic	34.9042	33.2256	31.7335	29.8033	36.3045	34.3904	32.5393	30.6701

Mean PSNR (dB) Per QP: Pixel-PAQ Versus IDSQ (YCbCr 4:2:2) – Random Access

Sequence	Pixel-PAQ				IDSQ			
	QP 22	QP 27	QP 32	QP 37	QP 22	QP 27	QP 32	QP 37
BirdsInCage	36.4532	35.5006	34.0949	32.1827	36.9894	36.4115	35.3608	33.9560
DuckAndLegs	29.1533	27.9895	26.7018	25.3548	30.2635	29.2285	27.7411	26.0493
Kimono	34.4255	33.2542	31.8061	30.1685	35.2015	34.1193	32.6956	31.1283
OldTownCross	31.4985	30.8881	29.9111	28.5249	31.8896	31.4928	30.6906	29.3754
ParkScene	32.1890	30.8004	29.3647	27.8868	33.4481	32.0739	30.4624	28.7974
Traffic	34.7826	32.6703	30.4097	28.1447	36.4386	34.3156	32.0356	29.5884

Mean PSNR (dB) Per QP: Pixel-PAQ Versus IDSQ (YCbCr 4:4:4) – Random Access

Sequence	Pixel-PAQ				IDSQ			
	QP 22	QP 27	QP 32	QP 37	QP 22	QP 27	QP 32	QP 37
BirdsInCage	34.5736	34.1050	33.2660	32.1066	34.7232	34.4621	33.9179	33.0211
DuckAndLegs	28.0381	27.0870	25.9042	24.6768	29.5056	27.9400	26.7760	25.2985
Kimono	33.7630	32.8515	31.6309	30.2587	34.1753	33.4081	32.2495	30.9117
OldTownCross	30.0597	29.6798	29.0180	28.0228	30.1151	29.9754	29.4715	28.5145
ParkScene	32.1325	30.8363	29.4403	28.0782	32.9975	31.8978	30.4856	28.8733
Traffic	34.8858	32.9088	30.8086	28.6553	36.2828	34.2486	32.0847	29.8005



Figure 14. The first intra-coded frame (AI QP = 22), coded by Pixel-PAQ, of the DuckAndLegs YCbCr 4:4:4 sequence.



Figure 15. The first intra-coded frame (AI QP = 22), coded by IDSQ, of the DuckAndLegs YCbCr 4:4:4 sequence.



Figure 16. The first frame of the raw DuckAndLegs YCbCr 4:4:4 sequence.

The plots in Figure 13 highlight the inferior PSNR results attained by Pixel-PAQ — compared with those achieved by IDSQ — on the DuckAndLegs 4:4:4 10-bit sequence. As previously mentioned, in spite of the very poor PSNR value of 28.04 dB attained by Pixel-PAQ on this sequence (in the RA QP = 22 test), as shown in Table 5, the compressed sequence is perceptually identical to the corresponding raw data (compare Figure 14 with Figure 16), as confirmed in the subjective evaluations.

Table 6. The criteria for quantifying the Mean Opinion Score (MOS) with respect to the visual reconstruction quality of a compressed video sequence compared with the raw video data.

MOS	Visual Quality Difference
5	Imperceptible (Visually Lossless)
4	Very Slightly Perceptible
3	Moderately Perceptible
2	Significantly Perceptible
1	Extremely Obvious

3.2 Subjective Visual Quality Evaluations

The subjective visual quality evaluations are undoubtedly the most important set of experiments in terms of measuring the perceptual quality of a compressed video sequence, especially for visually lossless coding and JND-based techniques. As regards the subjective evaluations conducted for the proposed Pixel-PAQ technique, the main objectives are as follows:

- To ascertain if Pixel-PAQ coded sequences differ from IDSQ coded sequences in terms of perceptual quality;
- To establish if Pixel-PAQ achieves visually lossless coding when comparing Pixel-PAQ coded sequences with the corresponding raw video data.

In the subjective evaluations, we follow, as closely as possible, the directions of the internationally standardised United Nations' ITU subjective assessments entitled *Subjective Video Quality Assessment Methods* (ITU-R Rec. P.910 [40]). As previously mentioned, the following conditions are recommended in ITU-R Rec. P.910:

- Number of participants ≥ 4 and ≤ 40 ;
- Viewing distance: $1.8 \times H$, where H is the height of the TV/VDU;
- Compute Mean Opinion Score (MOS);
- Spatiotemporal analysis.

The computer hardware in the experimental setup consists of a desktop PC which contains an Intel Core i7-4770 CPU — 4 cores and 8 threads — running at 3.4 GHz per core. The volatile memory in the PC is as follows: 24 GB of Double Data Rate (Type 3) Synchronous Dynamic Random Access Memory (DDR3 SDRAM) running at a DRAM frequency of 680 MHz. The Graphics Processing Unit (GPU) installed in the PC is an NVIDIA GeForce 750 Ti with a base core clock speed of 1020 MHz, a DDR5 SDRAM memory size of 2 GB and a memory bandwidth of 86.4 GHz/s. Note that the NVIDIA GeForce 750 Ti is a Ultra HD 4K and HDR-capable GPU that can support YCbCr 4:4:4 and RGB data of bit depths up to 12-bits per colour channel (i.e., 36-bits per pixel). Therefore, the higher dynamic ranges and also the lack of chroma subsampling in the raw 4:4:4 sequences are discernible (compared with the subsampled 4:2:0 8-bit sequences). The visual display hardware on which the subjective valuations are conducted is as follows: 1080p HD 32 Inch Samsung F5500 LED Smart TV/VDU.

In accordance with the conditions specified in the ITU-R Rec. P.910 [40] subjective evaluation procedures, four individuals participated in all tests; recall that ITU-R Rec. P.910 stipulates a minimum of four participants. Furthermore, the viewing distance of the participants from the TV/VDU is 1.5m in all evaluations ($1.5m \approx 59.1$ inch). Therefore, the height H of the TV/VDU is 15.7 inch and the viewing distance is approximately $4 \times H$.

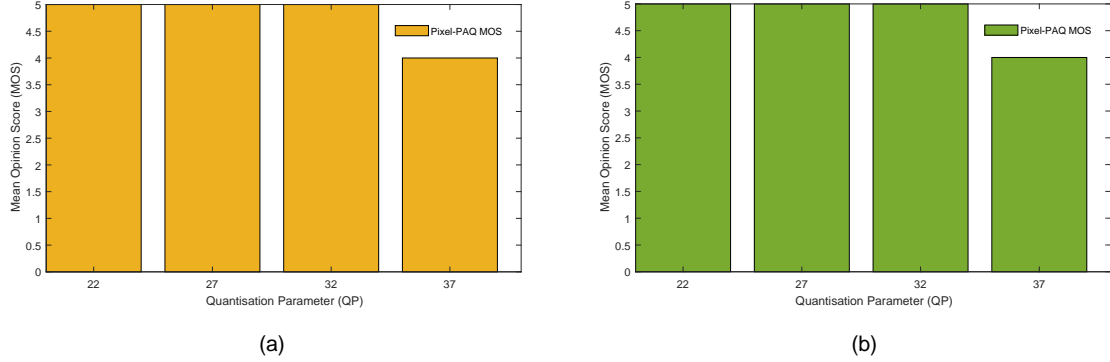


Figure 17. Two bar graphs which show the Mean Opinion Score (MOS) for the proposed technique over four QP data points (i.e., QPs 22, 27, 32 and 37). Subfigure (a) shows the MOS for Pixel-PAQ versus IDSQ on the BirdsInCage 4:4:4 10-bit sequence using the RA configuration. Subfigure (b) shows the MOS for Pixel-PAQ versus the raw video data on the Traffic 4:4:4 10-bit sequence.

Table 7. The MOS results, rounded to the nearest integer, of four participants in the subjective evaluations for Pixel-PAQ versus IDSQ. The sequences viewed are coded with initial QPs 22, 27, 32 and 37 on the YCbCr 4:2:0, 4:2:2 4:4:4 versions of the following sequences: BirdsInCage, DuckAndLegs Kimono, OldTownCross, ParkScene and Traffic compressed using the AI and RA configurations. The AI results are shown on the left; the RA results are shown on the right.

Rounded Mean Opinion Score (Spatiotemporal Subjective Evaluation) – Pixel-PAQ versus IDSQ

Sequence	YCbCr 4:2:0 All Intra				YCbCr 4:2:0 Random Access			
	QP 22	QP 27	QP 32	QP 37	QP 22	QP 27	QP 32	QP 37
BirdsInCage	5	4	4	3	5	5	5	5
DuckAndLegs	5	5	5	5	5	5	5	5
Kimono	5	5	5	4	5	5	5	4
OldTownCross	5	5	4	4	5	5	5	4
ParkScene	5	4	3	2	5	5	5	4
Traffic	5	5	5	4	5	5	5	5

Rounded Mean Opinion Score (Spatiotemporal Subjective Evaluation) – Pixel-PAQ versus IDSQ

Sequence	YCbCr 4:2:2 All Intra				YCbCr 4:2:2 Random Access			
	QP 22	QP 27	QP 32	QP 37	QP 22	QP 27	QP 32	QP 37
BirdsInCage	5	5	4	2	5	5	4	3
DuckAndLegs	5	5	4	3	5	5	4	3
Kimono	5	5	4	3	5	5	4	2
OldTownCross	5	4	3	2	5	5	4	3
ParkScene	5	5	3	2	5	5	4	2
Traffic	5	5	3	2	5	5	5	4

Rounded Mean Opinion Score (Spatiotemporal Subjective Evaluation) – Pixel-PAQ versus IDSQ

Sequence	YCbCr 4:4:4 All Intra				YCbCr 4:4:4 Random Access			
	QP 22	QP 27	QP 32	QP 37	QP 22	QP 27	QP 32	QP 37
BirdsInCage	5	5	4	3	5	5	5	4
DuckAndLegs	5	5	5	5	5	5	5	5
Kimono	5	5	5	4	5	5	5	4
OldTownCross	5	5	4	4	5	5	4	4
ParkScene	5	5	4	3	5	5	4	4
Traffic	5	5	4	3	5	5	4	4

Table 8. The MOS results, rounded to the nearest integer, of four participants in the subjective evaluations for Pixel-PAQ versus the raw data. The sequences viewed are coded with initial QPs 22, 27, 32 and 37 on the YCbCr 4:2:0, 4:2:2 4:4:4 versions of the following sequences: BirdsInCage, DuckAndLegs Kimono, OldTownCross, ParkScene and Traffic compressed using the AI and RA configurations. The AI results are shown on the left; the RA results are shown on the right.

Rounded Mean Opinion Score (Spatiotemporal Subjective Evaluation) – Pixel-PAQ versus Raw Data								
Sequence	YCbCr 4:2:0 All Intra				YCbCr 4:2:0 Random Access			
	QP 22	QP 27	QP 32	QP 37	QP 22	QP 27	QP 32	QP 37
BirdsInCage	4	3	2	2	5	4	4	3
DuckAndLegs	5	4	3	2	5	5	4	4
Kimono	4	4	3	2	5	4	3	2
OldTownCross	5	4	3	2	5	5	4	3
ParkScene	4	3	2	1	4	3	3	2
Traffic	5	5	4	2	5	5	4	4

Rounded Mean Opinion Score (Spatiotemporal Subjective Evaluation) – Pixel-PAQ versus Raw Data								
Sequence	YCbCr 4:2:2 All Intra				YCbCr 4:2:2 Random Access			
	QP 22	QP 27	QP 32	QP 37	QP 22	QP 27	QP 32	QP 37
BirdsInCage	4	3	2	1	5	4	3	2
DuckAndLegs	5	5	4	3	5	5	4	3
Kimono	5	4	2	1	5	4	3	2
OldTownCross	5	4	2	1	5	4	2	2
ParkScene	5	4	2	1	5	5	4	2
Traffic	5	4	3	2	5	5	4	2

Rounded Mean Opinion Score (Spatiotemporal Subjective Evaluation) – Pixel-PAQ versus Raw Data								
Sequence	YCbCr 4:4:4 All Intra				YCbCr 4:4:4 Random Access			
	QP 22	QP 27	QP 32	QP 37	QP 22	QP 27	QP 32	QP 37
BirdsInCage	4	3	2	1	5	4	3	2
DuckAndLegs	5	5	4	3	5	5	4	3
Kimono	5	4	3	2	5	5	4	3
OldTownCross	5	4	2	1	5	5	4	3
ParkScene	5	4	3	2	5	4	4	3
Traffic	5	5	4	2	5	5	4	4

The MOS results tabulated in Table 7 indicate that there are negligible perceptual differences between the Pixel-PAQ coded versions versus the IDSQ coded versions of the following YCbCr 4:2:0 (8-bit), 4:2:2 (10-bit) and 4:4:4 (10-bit) sequences: BirdsInCage, DuckAndLegs, Kimono, OldTownCross, ParkScene and Traffic. This consistently proved to be the case for the AI and RA QP = 22 and QP = 27 tests. In most of the Pixel-PAQ versus IDSQ AI QP = 37 tests, including the experiments undertaken on the BirdsInCage 4:4:4 and 4:2:2 sequences, the chrominance quantisation-induced distortions are noticeable in the versions coded by Pixel-PAQ. Due to the fact that BirdsInCage comprises a high level of saturation and also a combination of low variance and high variance Cb and Cr data, the coarser quantisation applied to the chroma Cb and Cr CBs by Pixel-PAQ is conspicuous in the AI QP = 37 tests. The most significant bitrate reduction achieved by Pixel-PAQ, in comparison with IDSQ, is attained on the 4:4:4 version of the BirdsInCage sequence (75% bitrate reduction in the RA QP = 22 test). Furthermore, visually lossless coding is accomplished in addition to achieving the vast bitrate reduction.

The data recorded in Table 8 tabulates the subjective evaluation MOS scores for the Pixel-PAQ coded sequences versus the raw video data. The goal in this set of subjective evaluations is to ascertain if Pixel-PAQ successfully achieves visually lossless coding. The subjective evaluation participants confirm that visually lossless coding is accomplished by Pixel-PAQ in the AI QP = 22 and RA QP = 22 tests in the vast majority of cases and, in some cases, in the AI QP = 27 and the RA QP = 27 tests. Irrespective of the SSIM and PSNR results tabulated in Table 2-Table 5, the perceptual quality of the sequences coded by Pixel-PAQ using the GOP-based (inter coding) Random Access encoding configuration is considerably superior to those coded using the All Intra (intra-only) encoding configuration. This is especially true according to the tests performed with the higher initial QP values (i.e., QPs 32 and 37). The main reason for this is because intra-only coding is a relatively primitive spatial image coding method that does not employ motion estimation, motion compensation, advanced motion vector prediction and bidirectional inter prediction. Coding with I-frames only does not take into account the temporal redundancies that exist between frames, which constitutes a major shortcoming of All Intra lossy coding. Conversely, motion data with GOP-based inter coding in HEVC can be signalled to the decoder with the utilisation of merge mode or by motion vector differences, picture reference indices and the direction of the inter prediction. With this in mind, in the sequences coded by Pixel-PAQ, the quantisation-induced compression artifacts proved to be vastly more conspicuous in all AI tests, especially so at initial QP = 37. As such, based on the subjective evaluation results, it can be inferred that GOP-based inter coding is considerably more effective than intra-only coding in JND-based lossy video coding applications (and also lossy video coding applications in general).

4.0 Conclusions

A novel CB-level, JND-based luma and chroma perceptual quantisation technique is proposed for HEVC (named Pixel-PAQ). Pixel-PAQ exploits HVS-based perceptual masking, whereby spatial CSF-based luminance masking and chrominance masking are employed to achieve JND-based perceptual quantisation and visually lossless coding. The QPs for the Y CB, the Cb CB and the Cr CB are perceptually increased in order to considerably reduce bitrates without incurring a conspicuous impact on the reconstruction quality of the compressed video data. In the subjective and objective evaluations, Pixel-PAQ is compared with a state-of-the-art JND-based perceptual quantisation technique based on luminance masking (named IDSQ). In comparison with IDSQ, Pixel-PAQ achieves vast bitrate reductions — of up to 75% (68.6% over four QP data points) — on the YCbCr 4:4:4 10-bit version of the BirdsInCage sequence. In addition to this, the subjective evaluations confirmed that visually lossless coding is achieved in almost all cases in which the initial QP = 22 (for both the AI and RA tests). This proved to be the case for the Pixel-PAQ versus IDSQ tests and also the Pixel-PAQ versus raw video data tests. Finally, no significant differences in encoding and decoding runtimes are observed for Pixel-PAQ versus IDSQ; Pixel-PAQ achieved marginal runtime reductions in all tests.

Acknowledgements

The author would like to sincerely thank Shevach Riabtsev — Senior Video Engineer at Beamr — for his valuable feedback. With Shevach’s extensive knowledge and experience in terms of working on state-of-the-art HEVC algorithms in addition to his contributions accepted by JCT-VC during the standardisation of HEVC, the valuable comments provided by Shevach are greatly appreciated by the author.

The author would also like to show gratitude to Victor Sanchez, who is presently acting as the author’s PhD supervisor in the Department of Computer Science at the University of Warwick. As first author, Victor has published several papers in high impact IEEE journals and major IEEE conferences on the topic of mathematically lossless intra prediction coding in HEVC.

References

- [1] H. R. Wu, A. R. Reibman, W. Lin, F. Pereira, and S. S. Hemami, "Perceptual Visual Signal Compression and Transmission," *Proc. IEEE*, vol. 101, no. 9, pp. 2025–2043, 2013.
- [2] M. Naccari and M. Mrak, "Perceptually Optimized Video Compression," *Elsevier Academic Press Library in Signal Processing (Image and Video Compression and Multimedia)*, vol. 5, pp. 155-196, 2014.
- [3] G. T. Fechner, "Elements of Psychophysics, Volume 1," (Translated by H.E. Adler), New York: Holt, Rinehart & Winston, 1860.
- [4] G. Sullivan, J-R. Ohm, W. Han and T. Wiegand, "Overview of the High Efficiency Video Coding (HEVC) Standard," *IEEE Trans. Circuits Syst. Video Technol.*, vol. 22, no. 12, pp. 1649-1668, 2012.
- [5] JCT-VC: ITU-T Rec. H.265/HEVC (version 3) | ISO/IEC 23008-2, Information technology – Coding of audio-visual objects," JCT-VC (ITU-T/ISO/IEC), 2015.
- [6] J. Lainema, F. Bossen, W-J. Han, J. Min and K. Ugur, "Intra Coding of the HEVC Standard," *IEEE Trans. Circuits Syst. Video Technol.*, vol. 22, no. 12, pp. 1792-1801, 2012.
- [7] K. Ugur, A. Alshin, E. Alshina, F. Bossen, W-J. Han, J-H. Park and J. Lainema, "Motion Compensated Prediction and Interpolation Filter Design in H.265/HEVC," *IEEE J. Sel. Topics Signal Process.*, vol. 7, no. 6, pp. 946-955, 2013.
- [8] M. Wein, "Residual Coding," in *High Efficiency Video Coding: Coding Tools and Specification*, Springer, 2015, pp. 205-227.
- [9] M. Budagavi, A. Fuldseth, G. Bjøntegaard, V. Sze and M. Sadafale, "Core Transform Design in the High Efficiency Video Coding (HEVC) Standard," *IEEE J. Sel. Topics Signal Process.*, vol. 7, no. 6, pp. 1649-1668, 2013.
- [10] V. Sze, M. Budagavi and G. J. Sullivan, "HEVC Transform and Quantization," in *High Efficiency Video Coding (HEVC): Algorithms and Architectures*, Springer, 2014, pp. 141-170.
- [11] V. Sze and M. Budagavi, "High Throughput CABAC Entropy Coding in HEVC," *IEEE Trans. Circuits Syst. Video Technol.*, vol. 22, no. 12, pp. 1778-1791, 2012.
- [12] Joint Collaborative Team on Video Coding (JCT-VC). JCT-VC HEVC HM Reference Software, HM 16.7 [Online]. Available: <http://hevc.hhi.fraunhofer.de/>
- [13] Y. Dodge, "Mean Squared Error," in *The Concise Encyclopedia of Statistics*, Springer, 2008, pp. 337-339.
- [14] G. J. Sullivan and T. Wiegand, "Rate-Distortion Optimization for Video Compression," *IEEE Signal Processing Magazine*, vol. 15, no. 6, pp. 74-90, 1998.
- [15] M. Karczewicz, Y. Ye and I. Chong, "Rate Distortion Optimised Quantization," in *ITU-T SG16/Q6 VCEG, Doc. VCEG-AH21*, Antalya, Turkey, 2008.
- [16] A. Norkin, G. Bjøntegaard, A. Fuldseth, M. Narroschke, M. Ikeda, K. Andersson, M. Zhou, and G. Auwera, "HEVC Deblocking Filter," *IEEE Trans. Circuits Syst. Video Technol.*, vol. 22, no. 12, pp. 1746–1754, 2012.
- [17] C. Fu, E. Alshina, A. Alshin, Y. Huang, C. Chen, C. Tsai, C. Hsu, S. Lei, J. Park, and W. Han, "Sample Adaptive Offset in the HEVC Standard," *IEEE Trans. Circuits Syst. Video Technol.*, vol. 22, no. 12, pp. 1755–1764, 2012.
- [18] J. L. Mannos and D. J. Sakrison, "The Effects of a Visual Fidelity Criterion of the Encoding of Images," *IEEE Trans. Information Theory*, vol. 20, no. 4, pp. 525–536, 1974.
- [19] C. H. Chou and Y. C. Li, "A Perceptually Tuned Subband Image Coder Based on the Measure of Just-Noticeable-Distortion Profile," *IEEE Trans. Circuits Syst. Video Technol.*, vol. 5, no. 6, pp. 467-476, 1995.
- [20] C. H. Chou and C. W. Chen, "A Perceptually Optimized 3-D Subband Codec for Video Communication Over Wireless Channels.," *IEEE Trans. Circuits Syst. Video Technol.*, vol. 6, no. 2, pp. 143-156, 1996.

- [21] A. J. Ahumada and H. A. Peterson, "Luminance-Model-Based DCT Quantization for Color Image Compression," *Proc. SPIE*, vol. 1666, pp. 365–374, 1992.
- [22] A. B. Watson, "DCTune: A Technique for Visual Optimization of DCT Quantization Matrices for Individual Images," *Int. Symp. Society for Information Display Digest of Technical Papers*, vol. 24. 1993, pp. 946–949.
- [23] X. Yang, W. S. Ling, Z. Lu, E. P. Ong, and S. Yao, "Just Noticeable Distortion Model and its Applications in Video Coding," *Elsevier Signal Processing: Image Communication*, vol. 20, no. 7, pp. 662-680, 2005.
- [24] Y. Jia, W. Lin, and A. A. Kassim, "Estimating Just-Noticeable Distortion for Video," *IEEE Trans. Circuits Syst. Video Technol.*, vol. 16, no. 7, pp. 820–829, 2006.
- [25] Z. Wei and K. N. Ngan, "Spatio-Temporal Just Noticeable Distortion Profile for Grey Scale Image/Video in DCT Domain," *IEEE Trans. Circuits Syst. Video Technol.*, vol. 19, no. 3, pp. 337–346, 2009.
- [26] Z. Chen and C. Guillemot, "Perceptually-Friendly H.264/AVC Video Coding Based on Foveated Just-Noticeable-Distortion Model," *IEEE Trans. Circuits Syst. Video Techn.*, vol. 20, no. 6, pp. 806-819, 2010.
- [27] M. Naccari and M. Mrak, "Intensity Dependent Spatial Quantization with Application in HEVC," *IEEE Int. Conf. Multimedia and Expo*, San Jose, CA, 2013, pp. 1-6.
- [28] Y. Zhang, M. Naccari, D. Agrafiotis, M. Mrak and D. Bull, "High Dynamic Range Video Compression Exploiting Luminance Masking," *IEEE Trans. Circuits Syst. Video Techn.*, vol. 26, no. 5, pp. 950-964, 2016.
- [29] X. Zhang, W. Lin, and P. Xue, "Improved Estimation for Just-Noticeable Visual Distortion," *Elsevier Signal Processing*, vol. 85, no. 4, pp. 795-808, 2005.
- [30] M. Naccari and F. Pereira, "Advanced H.264/AVC-Based Perceptual Video Coding: Architecture, Tools, and Assessment," *IEEE Trans. Circuits Syst. Video Techn.*, vol. 21, no. 6, pp. 766-782, 2011.
- [31] H. R. Wu and K. R. Rao, *Digital Video Image Quality and Perceptual Coding*, 2005, pp. 640.
- [32] G. Wang, Y. Zhang, B. Li, R. Fan and M. Zhou, "A fast and HEVC-compatible perceptual video coding scheme using a transform-domain Multi-Channel JND model," *Springer Multimedia Tools and Applications*, vol. 76, pp. 1-27, 2017.
- [33] K. T. Mullen, "The contrast sensitivity of human colour vision to red-green and blue-yellow chromatic gratings," *Journal of Physiology*, vol. 359, pp. 381-400, 1985.
- [34] M. Wein, "The Hybrid Video Coding Scheme," in *High Efficiency Video Coding: Coding Tools and Specification*, Springer, 2015, pp. 37-55.
- [35] D. Flynn, D. Marpe, M. Naccari, T. Nguyen, C. Rosewarne, K. Sharman, J. Sole and J. Xu, "Overview of the Range Extensions for the HEVC Standard: Tools, Profiles, and Performance," *IEEE Trans. Circuits Syst. Video Techn.*, vol. 26, no. 1, pp. 4-19, 2016.
- [36] D. Flynn, N. Nguyen, D. He, A. Tourapis, G. Cote and D. Singer, "RExt: CU-adaptive chroma QP offsets," in *Doc: JCT-VC O0044, 15th Meeting of JCT-VC*, Geneva, CH, 2013, pp. 1-4.
- [37] L. Prangnell, M. Hernández-Cabronero and V. Sanchez, "Coding Block-Level Perceptual Video Coding for 4:4:4 Data in HEVC," *IEEE Int. Conf. Image Processing*, Beijing, 2017 (In Press).
- [38] F. Bossen, "Common Test Conditions and Software Reference Configurations," in *Doc. JCT-VC L1100, 12th Meeting of JCT-VC*, Geneva, CH, 2013, pp. 1-4.
- [39] Z. Wang, A. C. Bovik, H. R. Sheikh, and E. P. Simoncelli, "Image Quality Assessment: From Error Visibility to Structural Similarity," *IEEE Trans. Image Processing*, vol. 13, no. 4, pp. 600-612, 2004.
- [40] ITU-R: Rec. P.910, "Subjective Video Quality Assessment Methods for Multimedia Applications," 2008.